agronomy

MDPI

Article

From Chloroplast to Tolerance: AhSNAT5-Mediated Melatonin Biosynthesis Confers Salt Stress Tolerance in Peanut

Qi Wang [1], Lihuan Liu [2], Fangyan Ma [1] and Guanchu Zhang [1,*]

[1] Shandong Peanut Research Institute, Qingdao 266100, China; wqi0309@126.com (Q.W.); mafangyan1998@163.com (F.M.)

[2] Comprehensive Security Center, Inner Mongolia Agriculture and Animal Husbandry Department, Hohhot 010011, China; 15148359124@163.com

* Correspondence: guanchuzhang@126.com

Abstract

Melatonin is a multifunctional molecule that modulates plant growth and abiotic stress responses, yet the serotonin N-acetyltransferase (*SNAT*) gene family, a key component of melatonin biosynthesis, has not been characterized in peanut (*Arachis hypogaea* L.). In this study, 11 *AhSNAT* genes were identified genome-wide. These genes encoded proteins of 195–289 amino acids harboring the conserved Acetyltransf_7 domain, and their promoters were rich in *cis*-acting elements that are sensitive to hormonal and stress signals. Phylogenetic and synteny analyses indicated that segmental duplication drove family expansion, and purifying selection has maintained their conserved functions. The profiling of gene expression revealed patterns specific to organs and inducible by salt, among which *AhSNAT5* was strongly and rapidly induced by salt stress. AhSNAT5 was localized to chloroplasts. Notably, overexpression of *AhSNAT5* in *Arabidopsis* increased endogenous melatonin content and enhanced salt tolerance, accompanied by reduced accumulation of reactive oxygen species (ROS) and malondialdehyde, and elevated activities of antioxidant enzymes. Conversely, virus-induced gene silencing (VIGS) of *AhSNAT5* in peanut decreased melatonin biosynthesis and aggravated salt sensitivity, and exogenous melatonin partially rescued these defects. Collectively, our findings identify AhSNAT5 as a key enhancer of salt tolerance and a potential candidate for genetic improvement of peanut.

Keywords: antioxidant system; *Arachis hypogaea*; melatonin; salt stress; serotonin N-acetyltransferase

Academic Editors: Li'na Yin, Maria Gerakari and Ilias Avdikos

Received: 16 November 2026
Revised: 25 November 2026
Accepted: 26 November 2026
Published: 29 November 2026

Copyright: © 2026 by the authors. Licensee MDPI, Basel, Switzerland. This article is an open access article distributed under the terms and conditions of the Creative Commons Attribution (CC BY) license.

1. Introduction

The salinization of soil is a major environmental challenge for agriculture, impacting over 800 million hectares globally and severely limiting crop growth, development, and yield [1,2]. Peanut is a globally important oilseed crop cultivated extensively in arid and semi-arid regions, where soil salinity progressively reduces seed germination, seedling establishment, photosynthesis, and ultimately pod yield [3]. In addition, peanut is vulnerable to excess sodium uptake, osmotic imbalance, and secondary oxidative stress, which collectively impair membrane integrity, photosynthetic efficiency, and cellular metabolism. Consequently, identifying key regulatory genes and exploring the molecular mechanisms of salt stress responses are critical for genetically improving salt tolerance in peanut.

The accumulation of reactive oxygen species (ROS), including superoxide anion

(O_2.-) and hydrogen peroxide (H_2O_2), is triggered by salt stress, causing oxidative damage to lipids, proteins, and DNA, and inducing programmed cell death [4]. Plants counteract ROS through a sophisticated antioxidant machinery comprising enzymatic components such as SOD, POD, and CAT, as well as non-enzymatic antioxidants [4]. Among the emerging protective molecules, melatonin (N-acetyl-5-methoxytryptamine) was first discovered in plants nearly three decades ago [5] and has attracted exceptional attention owing to its powerful and multi-target antioxidant capacity. Melatonin both scavenges ROS through cascade reactions and regulates antioxidant enzyme activities, ion homeostasis, stomatal movement, and stress-related gene expression [6,7]. The role of phytomelatonin as a signaling molecule in plant stress responses is further supported by the identification of PMTR1/CAND2 as a potential receptor in *Arabidopsis* [8]. The use of exogenous melatonin has been shown repeatedly to enhance salt tolerance in diverse crop species by restoring photosynthetic performance, maintaining K^+/Na^+ homeostasis, and reinforcing the antioxidant system [9,10].

Melatonin in plants is produced from tryptophan *via* a sequence of four enzymatic steps. Tryptophan is first decarboxylated to tryptamine by tryptophan decarboxylase (TDC), hydroxylated to serotonin by tryptamine 5-hydroxylase (T5H), then acetylated to N-acetylserotonin by serotonin N-acetyltransferase (SNAT), and finally methylated to melatonin by N-acetylserotonin O-methyltransferase (ASMT) [11–13]. The first plant SNAT was identified from the GCN5-related N-acetyltransferase (GNAT) superfamily in rice and demonstrated to catalyze the acetylation of serotonin as the penultimate step of melatonin biosynthesis [13]. Subsequent studies revealed that rice SNAT enzymes are localized in chloroplasts, the primary site of plant melatonin biosynthesis [14]. The identification and functional characterization of *SNAT* homologs have been carried out in many species, including grape [15], tomato [16], soybean [17], and cotton [18]. Increasing research shows that SNAT is crucial and frequently acts as a bottleneck in regulating melatonin levels and stress resistance. Overexpression of *SNAT* genes elevates endogenous melatonin levels and confers enhanced tolerance to cold and salinity in transgenic rice [19], *VvSNAT1* in transgenic *Arabidopsis* [15], and *SlSNAT* in tomato [16]. Conversely, silencing of *GhSNAT3D* in cotton reduced melatonin content, antioxidant enzyme activities, and salt tolerance, and these defects were restored by exogenous melatonin supplementation [18]. These findings collectively establish *SNAT* genes as prime genetic targets for improving resistance through the regulation of melatonin biosynthesis.

The release of the reference genome of cultivated peanut has enabled systematic family-level analyses in this species. Although melatonin has been shown to alleviate salt-induced oxidative damage in peanut seedlings and melatonin biosynthesis-related genes such as *ASMT*, *TDC*, and *T5H* have been phylogenetically analyzed [3]. However, the *SNAT* gene family in peanut remains entirely unexplored, and the functions of specific *AhSNAT* genes in coping with salt stress are still unknown. In the present study, the *SNAT* gene family in peanut was identified and characterized on a genome-wide scale. A total of 11 *AhSNAT* genes were identified and analyzed with respect to phylogenetic relationships, chromosomal distribution, gene structure, conserved motifs, protein physicochemical properties, tertiary structure, cis-acting elements, and synteny among peanut, *Arabidopsis*, soybean, and rice. Transcriptome-based expression profiling and qRT-PCR were employed to investigate the organ-specific and salt-responsive expression patterns, leading to the selection of *AhSNAT5* for further functional analysis. Subcellular localization revealed that *AhSNAT5* resides in chloroplasts. *Arabidopsis* plants with overexpressed *AhSNAT5* showed improved salt tolerance by promoting melatonin accumulation, reducing ROS accumulation, and strengthening antioxidant capacity. Whereas VIGS-mediated silencing of *AhSNAT5* in peanut compromised salt tolerance, an effect

that was rescued by exogenous melatonin. Our findings systematically characterize the *SNAT* gene family in peanuts and highlight *AhSNAT5* as a potential candidate for molecular breeding to improve salt tolerance in peanuts. Here, our working hypothesis was that peanut chloroplast-localized AhSNAT family members, especially salt-induced *AhSNAT5*, positively mediate melatonin biosynthesis and improve salt resistance by mitigating salt-triggered oxidative damage.

2. Materials and Methods

2.1. Plant Materials and Growth Conditions

Huayu 9301 (a salt-tolerant variety developed by our team) peanut seeds were sterilized on the surface using 75% ethanol for 1 min and 0.1% $HgCl_2$ for 10 min, followed by five rinses with sterile distilled water. The germination of seeds was carried out in Petri dishes with moist filter paper at 25 °C in the dark for 48 h. Seedlings that had fully germinated were moved into plastic pots (10 cm × 10 cm) containing nutrient soil and vermiculite and cultivated in a growth chamber with a 16 h light (100 μmol m^{-2} s^{-1}) and 8 h dark cycle at 25 °C for both day and night. *Nicotiana benthamiana* plants used for subcellular localization were grown under identical conditions for 4–5 weeks before agroinfiltration. *Arabidopsis* (Col-0) was used as the wild type (WT) for genetic transformation, and seedlings were grown on 1/2 MS medium or in soil under a 16 h light (100 μmol m^{-2} s^{-1}) and 8 h dark cycle at 22 °C.

2.2. Genome-Wide Identification of the AhSNAT Gene Family

The peanut genome was downloaded from PeanutBase. To identify SNAT family members, the HMM profile of the Acetyltransf_7 domain (PF07247) was retrieved from the Pfam database [20], and the peanut proteome was searched using HMMER software (version 3.0) (E-value = 1×10^{-5}) [21]. BLASTp 2.2.28 searches utilized *Arabidopsis* SNAT protein sequences as query inputs (E-value = 1×10^{-10}). After merging sequences from both approaches, redundant entries were deleted. The complete Acetyltransf_7 domain in each candidate was validated using the NCBI-CDD [22] and SMART [23]. The final 11 *AhSNAT* genes were sequentially named *AhSNAT1-AhSNAT11* according to their physical positions on the chromosomes.

2.3. Physicochemical Properties and Phylogenetic Analysis

The ExPASy ProtParam online platform was utilized to compute fundamental physicochemical characteristics of individual AhSNAT proteins, such as coding sequence length, amino acid count, *MW*, and *pI* [24]. Plant-mPLoc was used to predict subcellular localization [25]. AhSNAT proteins were aligned using MAFFT(version 7.520) with its default settings for multiple sequence alignment [26]. Phylogenetic relationships were inferred via the neighbor-joining (NJ) algorithm in MEGA 6 [27]. Tree reconstruction was performed using the Poisson substitution model, with pairwise deletion of missing data and 1000 bootstrap resampling iterations.

2.4. Protein Tertiary Structure Prediction and Conserved Motif Analysis

AlphaFold2 (https://alphafold.ebi.ac.uk/) was used to predict the 3D structure of AhSNAT5, with pLDDT metrics serving as a measure of the trustworthiness of the predicted conformations. Conserved peptide signatures were uncovered with the MEME suite (https://meme-suite.org/meme/tools/meme, accessed on 20 July 2026), applying configuration settings limiting motif counts up to 10, alongside a 6-residue lower bound and 50-residue upper bound for motif dimensions. Sequence logos of conserved motifs within the Acetyltransf_7 domain were generated using WebLogo.

2.5. Gene Structure and CRE Analysis

GSDS 2.0 generated schematic depictions of *AhSNAT* exon-intron structures by matching coding regions to their genomic sequences. For *cis*-acting regulatory element (CRE) analysis, the 2000 bp upstream genomic sequences from the translation start position of each *AhSNAT* gene were retrieved and analyzed using the PlantCARE database to predict CREs. Identified CREs were categorized and visualized based on their functional annotations.

2.6. Chromosomal Distribution, Gene Duplication, and Collinearity Analysis

The chromosomal positions of *AhSNAT* genes were obtained from the peanut genome annotation file and graphically exhibited *via* TBtools software Version 2.210 [28]. Genome-wide duplication patterns among *AhSNAT* homologs were screened using MCScanX v1.0.0 under default operational settings [29]. The DnaSP 5.0 program [30] was utilized to estimate *Ka* and *Ks* substitution ratios of segmentally and tandemly duplicated gene pairs. For collinearity analysis, genome sequences and annotation files of *Arabidopsis*, soybean, and rice were acquired from Ensembl Plants, and the identification and visualization of collinear relationships were performed using the Dual Synteny Plotter in TBtools [28].

2.7. Expression Pattern Analysis and qRT-PCR

Expression data of *AhSNAT* genes across multiple peanut organs (leaves, peg tips, floral organs, roots, nodules, developing seeds, etc.) were obtained from the PeanutBase transcriptome database. For salt-responsive expression analysis, RNA-seq data of peanut roots under 200 mM NaCl treatment at different time points were retrieved from NCBI (accession number PRJNA1309984). Transcript abundance was normalized and hierarchically clustered, and heatmaps were generated with TBtools [28].

To validate qRT-PCR, total RNA was isolated from peanut or *Arabidopsis* tissues using the RNA extraction kit following the manufacturer's instructions. First-strand cDNA synthesis was performed using 1 μg total RNA with the PrimeScript RT Reagent Kit with gDNA Eraser (Takara, Dalian, China). Using TB Green Premix Ex Taq II (Takara Dalian, China), qRT-PCR was carried out on a CFX96 Real-Time PCR Detection System (Bio-Rad, Hercules, CA, USA) in a reaction volume of 20 μL. The peanut *AhActin* and *Arabidopsis AtActin2* served as endogenous controls for transcript quantification, respectively [31,32]. Relative gene expression levels were calculated using the $2^{-\Delta\Delta Ct}$ method [33], with three biological replicates and three technical replicates for each experiment. Primer sequences are listed in Supplementary Table S1.

2.8. Subcellular Localization of AhSNAT5

The CDS of *AhSNAT5*, excluding the stop codon, was amplified and inserted in-frame into the pCHF3-cGFP vector under the control of the 35S promoter to create the *35S::AhSNAT5-GFP* fusion construct. After confirmation by sequencing, the construct was inserted into *Agrobacterium* strain GV3101 by the freeze–thaw transformation method. *Agrobacterial* suspensions were resuspended in infiltration buffer to an OD600 of 0.6, incubated for 2 h at room temperature in darkness, and infiltrated into fully expanded *N. benthamiana* leaves. At 3 days post-infiltration, GFP fluorescence and chlorophyll autofluorescence were visualized with a confocal microscope, and images were merged to analyze the subcellular localization.

2.9. Overexpression of AhSNAT5 in Arabidopsis and Salt Stress Assay

The CDS of *AhSNAT5* was inserted into the binary vector pCHF3 downstream of the

35S promoter to construct the *35S::AhSNAT5* overexpression vector. *Arabidopsis* Col-0 plants were treated with the construct *via* the floral dip method after it was transformed into *Agrobacterium* strain GV3101 [34]. Homozygous T3 lines were acquired after selecting transgenic seeds on 1/2 MS medium with 25 mg/L hygromycin. Two independent homozygous lines with high *AhSNAT5* expression (*AhSNAT5-OE1* and *AhSNAT5-OE5*), verified by qRT-PCR, were selected for functional analysis.

For salt stress assays, 3-week-old WT and overexpression seedlings cultivated in soil were watered with a 150 mM NaCl solution [35], while control plants were given an equal volume of water. Each pot was irrigated with 50 mL of 150 mM NaCl solution every two days for a total 10-day treatment period. After 10 days of treatment, phenotypic images were recorded, and the survival rates and growth performance were evaluated. Seedlings with >50% green rosette leaf area were counted as surviving individuals for survival-rate statistics. Rosette leaves of WT and *OE* lines under control and salt stress conditions were harvested for the determination of melatonin content, ROS accumulation, TBARS content, and antioxidant enzyme activities.

2.10. Virus-Induced Gene Silencing (VIGS) in Peanut

A TRV-based VIGS system was used to silence *AhSNAT5* in peanut. A 300 bp *AhSNAT5*-specific fragment was amplified from the coding sequence and ligated into pTRV2, yielding the recombinant vector *pTRV2-AhSNAT5*. The empty pTRV2 vector, designated *TRV-00*, was employed as the negative control. All recombinant vectors were transformed into *Agrobacterium* strain GV3101. *Agrobacterial* suspensions carrying pTRV1 and pTRV2-derived constructs were mixed at a 1:1 ratio, incubated for 2 h at room temperature in darkness, and infiltrated into the cotyledons and first true leaves of 7-day-old peanut seedlings with a needleless syringe. Plants were cultivated in growth chambers set to a 16 h light/8 h dark cycle at a constant temperature of 22 °C. The silencing efficiency of *AhSNAT5* in agroinfiltrated plants was quantified by qRT-PCR one week post-infiltration; individuals with confirmed knockdown of *AhSNAT5* were selected for downstream analyses.

2.11. Exogenous Melatonin Rescue Assay and Melatonin Content Determination

For the melatonin rescue assay, leaf discs (1 cm in diameter) were punched from fully expanded leaves of *TRV-00* and *TRV-AhSNAT5* seedlings and floated in Petri dishes containing 20 mL of test solution under three conditions: (1) control (distilled water), (2) 200 mM NaCl, and (3) 200 mM NaCl + 25 μM melatonin (MT) [36,37]. The melatonin-only treatment group was not included; preliminary observations indicated that 25 μM exogenous melatonin did not produce obvious phenotypic or physiological alterations in peanut leaf discs under non-saline control conditions. All Petri dishes were incubated in a growth chamber maintained at 25 °C under a 16 h light/8 h dark cycle for a period of 7 days. Phenotypic images were captured after treatment, and leaf discs were collected for the measurement of chlorophyll content, *Fv/Fm* ratio, electrolyte leakage, TBARS content, and antioxidant enzyme activities.

For endogenous melatonin quantification, fresh leaves (0.1 g) of WT, *AhSNAT5-OE*, *TRV-00*, and *TRV-AhSNAT5* plants were harvested, immediately frozen in liquid nitrogen, and ground into powder. Melatonin was extracted with methanol and quantified by ultra-performance liquid chromatography coupled with the UPLC-MS/MS method.

2.12. Measurements of Physiological and Biochemical Indicators

The *Fv/Fm* was measured on individual leaves using a chlorophyll fluorometer according to the manufacturer's instructions. Chlorophyll extraction was performed on 0.1

g aliquots of fresh leaf tissue with 10 mL of 80% acetone under dark conditions at 4 °C for 24 h, followed by spectrophotometric determination of absorbance at 645 and 665 nm. Total chlorophyll content was calculated as: chlorophyll (mg/g FW) = (20.29 D645 + 8.04 D665) × V/(1000 × W), where D is the optical density at the indicated wavelength, V is the total extraction volume (mL), and W is the fresh weight (g) [32]. For electrolyte leakage, freshly harvested leaves were submerged in deionized water and agitated at 25 °C for 30 min; the first conductivity reading (C1) was then obtained using a conductivity meter. The tissues were then subjected to boiling treatment for 10 min to achieve complete membrane disruption, whereupon the final conductivity (C2) was determined. The relative electrolyte leakage (%) was calculated using the following formula: C1/C2 × 100.

The contents of O_2·-, H_2O_2, and TBARS, as well as the activities of SOD, POD, and CAT, were determined using corresponding commercial assay kits following the manufacturer's protocols. O_2·- was measured based on nitrite formation from the hydroxylamine reaction; H_2O_2 content was quantified via the titanium-peroxide complex color reaction. SOD activity was assayed by the nitroblue tetrazolium photoreduction inhibition method; POD activity was determined by monitoring guaiacol oxidation rate; CAT activity was measured by detecting H_2O_2 decomposition rate. TBARS (thiobarbituric acid-reactive substances) was quantified by the thiobarbituric acid colorimetric reaction; note that this assay detects total thiobarbituric acid-reactive substances rather than MDA specifically. All biochemical measurements were performed with three independent biological replicates.

2.13. Statistical Analysis

All experiments included at least three independent biological replicates, and the results are expressed as the mean ± standard deviation (SD). Statistical analyses were performed in GraphPad Prism 8, with differences between two groups assessed by Student's *t*-test and multiple comparisons conducted by one-way ANOVA followed by Tukey's post hoc test. Differences were considered statistically significant at $p < 0.05$, and lowercase letters above the bars denote values that differ significantly at the 0.05 level.

3. Results

3.1. Genome-Wide Identification and Conserved Domain Analysis

Genome-wide HMMER and BLASTp 2.2.28 screening against the Acetyltransf_7 domain (PF07247) identified 11 *AhSNAT* genes from the peanut genome, designated *AhSNAT1-AhSNAT11* by chromosomal positions (Supplementary Table S2). CDS lengths ranged from 588 to 870 bp, encoding 195–289 amino acids with molecular weights of 21.73–31.79 kDa and pI 5.20–9.95. Subcellular prediction indicated multiple organelle targets, with most isoforms localized to chloroplasts, consistent with the primary site of plant melatonin biosynthesis. Multiple sequence alignment confirmed a conserved Acetyltransf_7 domain in each AhSNAT protein, containing highly conserved catalytic residues (Figure 1A). AlphaFold tertiary structure prediction showed high pLDDT confidence in the core domain, while N- and C-terminal regions had low reliability. WebLogo revealed conserved β-sheet and α-helix signatures within the core acetyltransferase motif (Figure 1B). Phylogenetic analysis of peanut and *Arabidopsis* SNATs grouped AhSNAT paralogs into subclades, with several clustering closely with AtSNATs, indicating evolutionary conservation across dicots (Figure 1C).

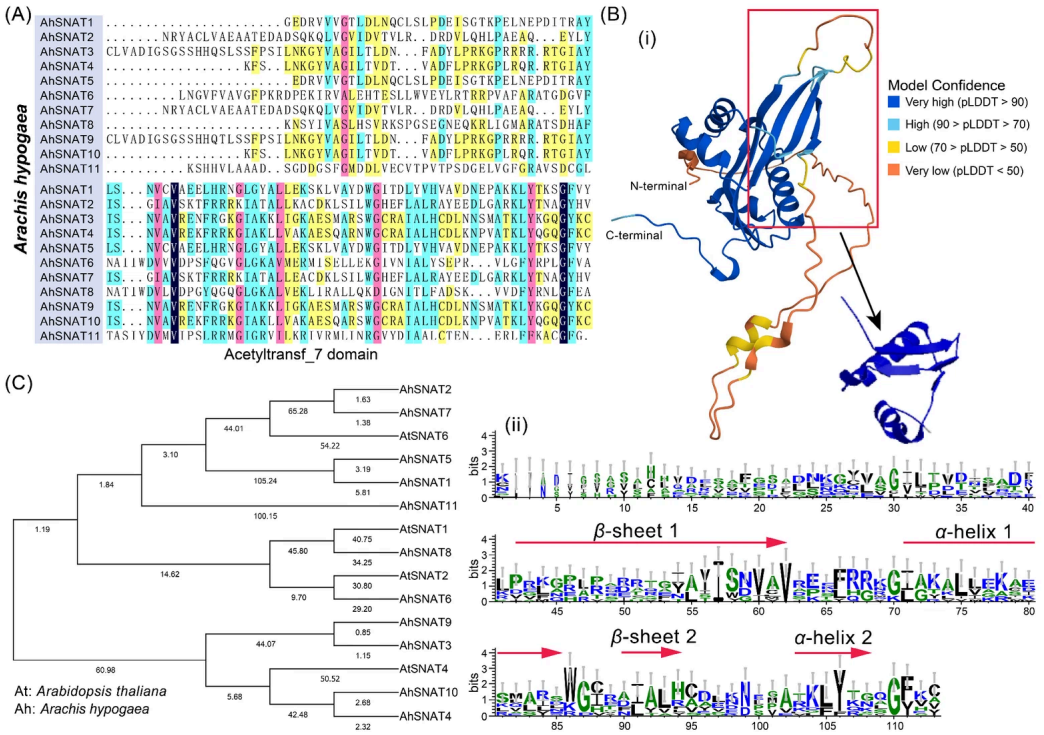


Figure 1. Sequence characterization, protein structural prediction, and phylogenetic analysis of the AhSNAT family in peanut. (**A**) Multiple-sequence alignment of 11 AhSNAT proteins. The conserved Acetyltransf_7 domain is highlighted. Conserved amino acid residues are color-coded. (**B**) Predicted tertiary structure of the AhSNAT protein. (**i**) Protein model confidence is indicated by pLDDT-based color coding. The red box marks the Acetyltransf_7 functional domain. (**ii**) Sequence logos of conserved motifs within the Acetyltransf_7 domain, with annotated secondary-structure elements (*β*-sheet and *α*-helix). (**C**) Phylogenetic tree of SNAT proteins from peanut (*Arachis hypogaea*, Ah) and *Arabidopsis thaliana* (At). Bootstrap values are shown on each branch.

3.2. Gene Structure, Conserved Motifs and CRE Analysis of AhSNATs

To investigate structural characteristics and regulatory mechanisms of peanut *SNAT* genes, we analyzed exon-intron organization and conserved motifs. Gene-structure analysis showed members within the same phylogenetic clade had highly similar exon-intron arrangements, while substantial divergence occurred among distinct clades (Figure 2A). Most *AhSNAT* genes contained multiple exons interrupted by introns, with variations in intron number and gene length. Conserved-motif prediction identified ten distinct motifs (1–10). Among these, motif 1 corresponded to the Acetyltransf_7 domain and was present in all AhSNAT proteins. Closely related paralogs shared comparable motif composition and order, implying functional conservation (Figure 2B).

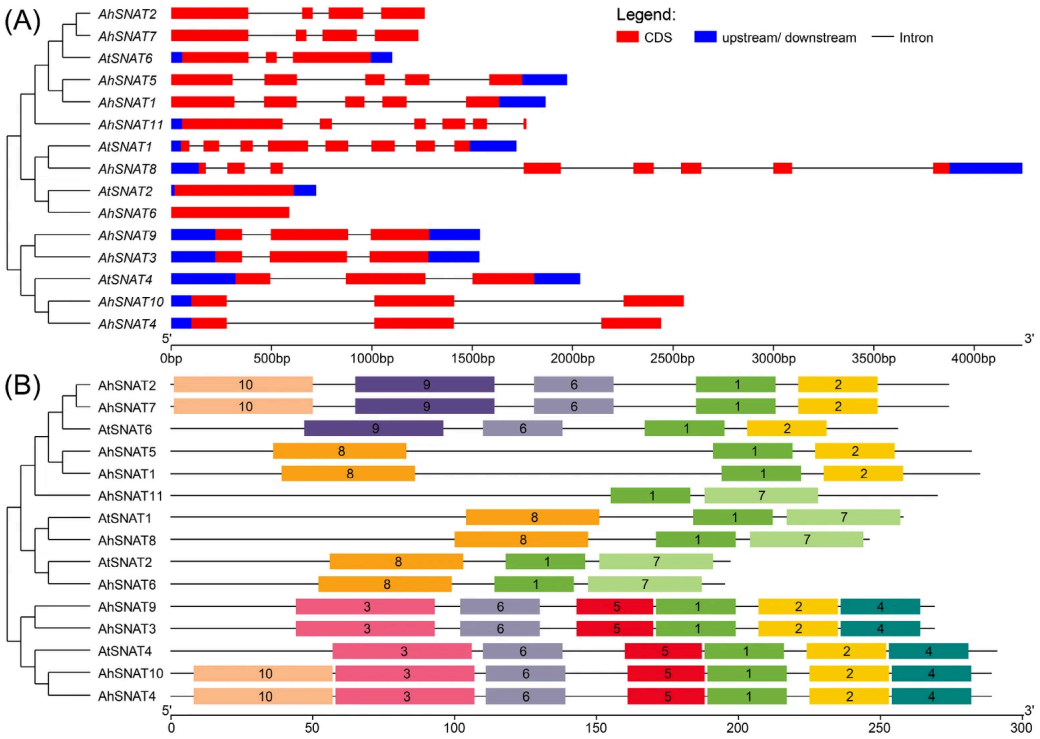


Figure 2. Schematic characterization of gene architectures and conserved peptide signature of AhSNAT members. (**A**) Exon-intron arrangements of *AhSNAT* genes. Red boxes represent coding sequence (CDS) regions; blue boxes indicate upstream/downstream sequences; black horizontal lines denote introns. (**B**) Distribution of ten conserved protein motifs among AhSNAT proteins. Different colored boxes correspond to distinct conserved motifs.

3.3. Chromosomal Distribution, Duplication and Evolutionary Analysis

Chromosomal localization analysis revealed that the 11 *AhSNAT* genes were non-uniformly distributed across 10 chromosomes of the peanut genome (Figure 3A). Nine chromosomes, namely chromosomes 1, 3, 5, 9, 11, 14, 15, 19, and 20, each carried a single *AhSNAT* gene, whereas chromosome 13 accommodated two, reflecting a scattered distribution pattern. Gene duplication analysis revealed four segmental duplication events (*AhSNAT1/5*, *2/7*, *3/9*, *4/10*) driving family expansion, with no tandem duplications detected (Supplementary Table S3). *Ka*/*Ks* ratios < 1 for all duplicated *AhSNAT* gene pairs indicated purifying selection maintained conserved SNAT catalytic functions. Cross-species collinearity analysis among peanut, *Arabidopsis*, soybean, and rice detected extensive collinear relationships between peanut and soybean but fewer orthologous blocks between peanut and *Arabidopsis* or rice (Figure 3B, Supplementary Table S4). These results are consistent with closer phylogenetic affinity between leguminous species (peanut and soybean) than cruciferous (*Arabidopsis*) or gramineous (rice) species.

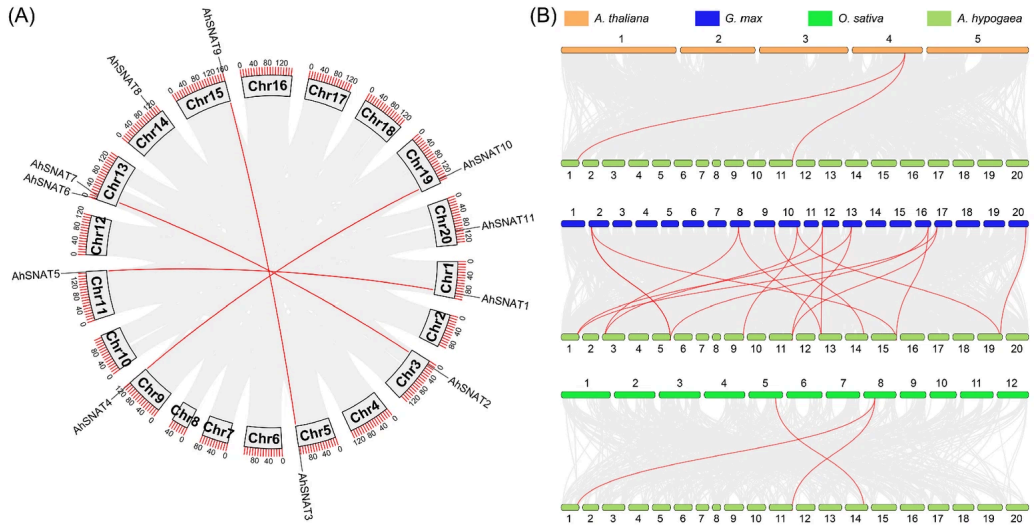


Figure 3. Chromosomal localization and collinearity analysis of *AhSNAT* genes. (**A**) Distribution of 11 *AhSNAT* genes on peanut chromosomes. Chromosome numbers are labeled, and the scale bars on each chromosome represent physical positions (in Mb). Red lines link duplicated *AhSNAT* gene pairs. (**B**) Collinearity analysis of *SNAT* genes among *Arabidopsis thaliana* (orange), *Glycine max* (blue), *Oryza sativa* (green), and *Arachis hypogaea* (light green). Chromosome numbers are indicated for each species, and collinear *SNAT* pairs between species are linked by red lines.

3.4. Promoter Analysis

To explore the possible transcriptional regulation of the peanut *AhSNAT* genes, the 2.0 kb sequences upstream of the ATG start codon were retrieved for all 11 members and interrogated against the PlantCARE database for *cis*-acting regulatory elements. The results showed that the numbers, types, and positions of *cis*-acting elements varied considerably among the 11 *AhSNAT* promoters, suggesting functional divergence among the members of this gene family (Figure 4). Notably, *AhSNAT1*, *AhSNAT3*, and *AhSNAT9* harbored abundant MeJA-responsive elements, with multiple clustered motifs distributed across their promoters, implying that these genes may be strongly regulated by jasmonate signaling. In contrast, the promoters of *AhSNAT2*, *AhSNAT4*, and *AhSNAT7* contained multiple ABA-responsive elements, indicating that ABA signaling likely participates in the transcriptional regulation of these genes. In addition, anaerobic induction elements were widely distributed in the promoters of most *AhSNAT* members, particularly in *AhSNAT2*, *AhSNAT3*, *AhSNAT5*, and *AhSNAT9*, whereas WUN motifs were enriched in *AhSNAT7* and *AhSNAT9*, suggesting their potential involvement in wound responses. Drought-inducibility and low-temperature responsiveness elements (MBS and LTR) were also detected in several promoters, including *AhSNAT4*, *AhSNAT8*, and *AhSNAT10*, hinting at roles for the corresponding genes in drought and cold stress responses.

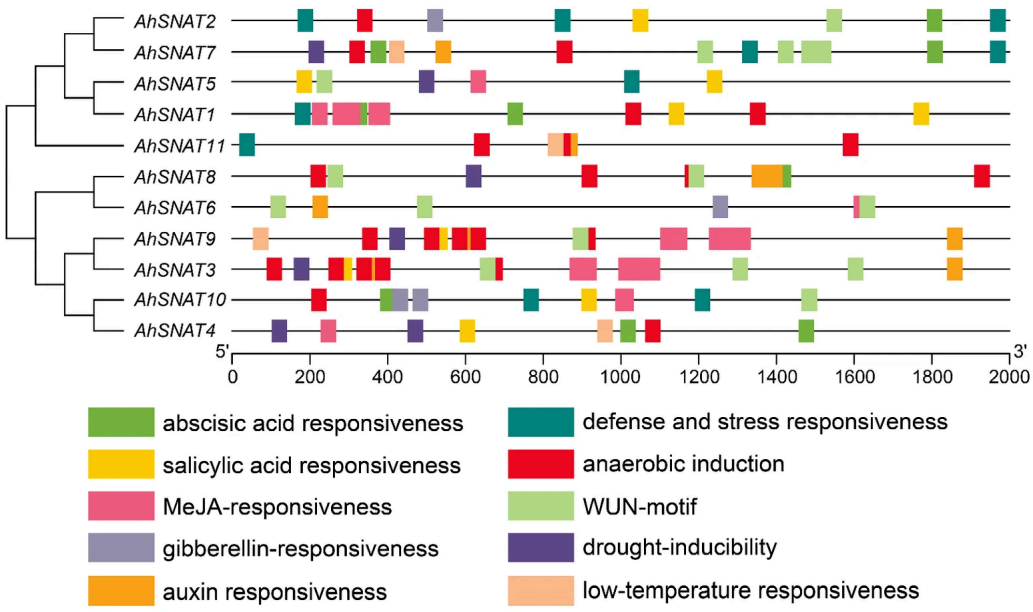


Figure 4. *Cis*-acting element analysis of the promoters of peanut *AhSNAT* genes.

3.5. Expression Pattern Analysis

To dissect the spatial-temporal expression profiles of *AhSNAT* family members, two transcriptome-derived heatmaps were generated. The organ-specific expression heatmap exhibited divergent transcript patterns for *AhSNAT* genes across multiple peanut organs, including leaves, peg tips, floral organs, roots, nodules, and developing seeds (Figure 5A). Several *AhSNAT* genes displayed organ-preferential expression. Notably, *AhSNAT5* showed relatively high basal transcript abundance in roots, which represent the primary organ for sensing soil salinity.

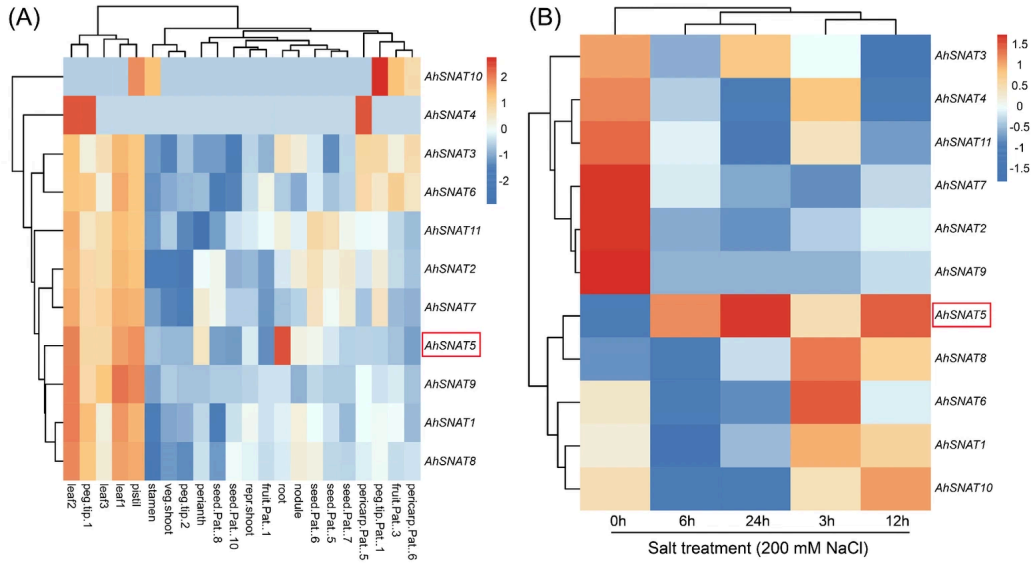


Figure 5. Organ-specific and salt-responsive expression patterns of *AhSNAT* family genes in peanut. (**A**) Heatmap illustrating the organ-specific transcript abundance of *AhSNAT* genes across diverse peanut organs and developmental stages. The color gradient represents normalized transcript levels. (**B**) Time-course expression profiles of *AhSNAT* genes under 200 mM NaCl salt treatment (0, 3, 6, 12, 24 h). The red box highlights *AhSNAT5*, which is markedly induced by salt stress. Hierarchical clustering was performed for both rows and columns. The color scale denotes nor-

malized gene expression values.

Under 200 mM NaCl salt stress, the *AhSNAT* paralogs exhibited distinct time-dependent expression dynamics (Figure 5B). A subset of *AhSNAT* genes were rapidly induced within 6–24 h following salt exposure, whereas others were transcriptionally repressed. Importantly, *AhSNAT5* was strongly up-regulated upon salt treatment, showing prominent transcript elevation at 3, 6, 12, and 24 h under salinity stress. This observation implied that *AhSNAT5* is a salt-responsive gene of the AhSNAT family and may participate in peanut adaptation to high-salt environments.

3.6. qRT-PCR and Subcellular Localization of AhSNAT5

The expression patterns of five selected genes (*AhSNAT1*, *AhSNAT5*, *AhSNAT6*, *AhSNAT8*, and *AhSNAT10*) were examined by qRT-PCR at 0, 1, 3, and 6 h after salt exposure (Figure 6A). All five genes responded to salt treatment, but with distinct temporal profiles. *AhSNAT5* was strongly and rapidly induced, with its transcript level increasing to approximately 6.9-fold at 1 h and reaching a maximum of approximately 8.8-fold at 3 h, followed by a decline at 6 h. Similarly, *AhSNAT6* and *AhSNAT8* exhibited a transient induction pattern, with the highest transcript level at 1 h and 3 h, respectively. *AhSNAT10* was progressively up-regulated during the treatment, peaking at 6 h with an approximately 3.4-fold increase. These results indicate that the selected *AhSNAT* genes are differentially regulated by salt stress, among which *AhSNAT5* displayed the most pronounced and sustained transcriptional response. Given its prominent transcriptional responsiveness, AhSNAT5 was selected for subcellular localization analysis (Figure 6B). The coding sequence of *AhSNAT5* was fused in-frame to the green fluorescent protein (GFP) reporter and transiently expressed in tobacco leaves. The results indicated that the GFP fluorescence of the AhSNAT5-GFP fusion protein overlaps with the spontaneous fluorescence of chlorophyll in chloroplasts, indicating that AhSNAT5 is localized to chloroplasts.

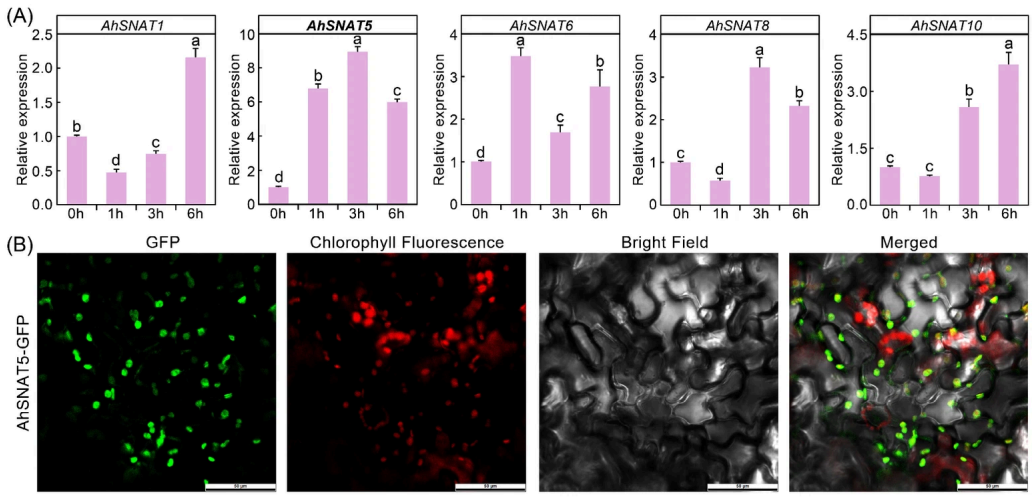


Figure 6. Expression analysis of selected *AhSNAT* genes and subcellular localization of the AhSNAT5 protein. (**A**) qRT-PCR analysis of *AhSNAT1*, *AhSNAT5*, *AhSNAT6*, *AhSNAT8*, and *AhSNAT10* expression at 0, 1, 3, and 6 h after salt treatment. Relative transcript levels were quantified by the $2^{-\Delta\Delta Ct}$ method based on three biological replicates, and the results are shown as the mean ± SD. Different lowercase letters above the bars denote significant differences (one-way ANOVA with Tukey's post hoc test, $p < 0.05$). (**B**) Localization of AhSNAT5-GFP in *Nicotiana benthamiana* leaves after transient expression, observed by confocal microscopy. Scale bars = 50 μm.

3.7. Overexpression of AhSNAT5 Enhances Salt Stress Tolerance in Arabidopsis

To investigate the functional role of *AhSNAT5* in salt stress tolerance, two independent overexpression lines (*AhSNAT5-OE1* and *AhSNAT5-OE5*) were generated in *Arabidopsis* (Col-0), and the transcript levels of *AhSNAT5* were verified by qRT-PCR (Figure 7A). Consistent with the enhanced *AhSNAT5* expression, the melatonin contents of the *OE* lines were significantly higher than those of WT. These results indicate that overexpression of *AhSNAT5* effectively promotes melatonin biosynthesis in *Arabidopsis* (Figure 7B). To evaluate salt stress tolerance, three-week-old WT and *OE* seedlings were subjected to salt stress treatment. Before treatment, no obvious morphological differences were observed among the genotypes. After salt stress, however, the WT plants exhibited severe wilting and chlorosis, whereas both *OE* lines displayed markedly greener leaves and better growth performance (Figure 7C), demonstrating that *AhSNAT5* overexpression enhances salt stress tolerance.

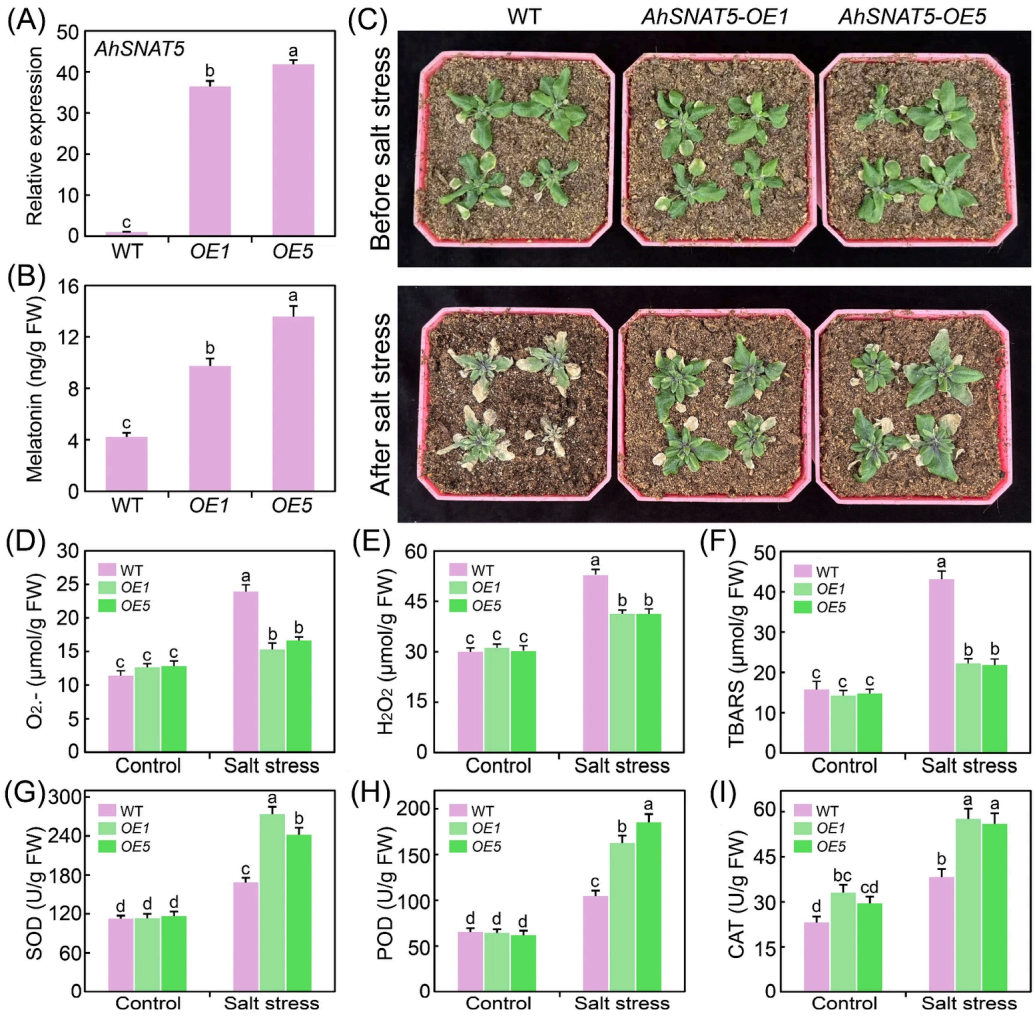


Figure 7. Functional verification of *AhSNAT5* overexpression in *Arabidopsis* under salt stress. (**A**) Relative expression levels of *AhSNAT5* in the wild type (WT) and two independent overexpression lines (*OE1* and *OE5*), determined by qRT-PCR. (**B**) Melatonin contents in WT and *OE* lines. (**C**) Phenotypes of WT and *AhSNAT5*-overexpression plants before and after salt stress (150 mM NaCl) treatment. (**D**–**F**) Contents of superoxide anion (O_2.-) (**D**), hydrogen peroxide (H_2O_2) (**E**), and thiobarbituric acid-reactive substances (TBARS) (**F**) in WT and *OE* lines under control and salt stress conditions. (**G**–**I**) Activities of superoxide dismutase (SOD) (**G**), peroxidase (POD) (**H**), and catalase (CAT) (**I**) in WT and *OE* lines under control and salt stress conditions. FW, fresh weight. The

results are shown as the mean ± SD of three biological replicates. Different lowercase letters above the bars denote significant differences (one-way ANOVA with Tukey's post hoc test, $p < 0.05$).

Furthermore, no significant differences in O_2.-, H_2O_2, or TBARS contents were detected among genotypes under control conditions. After salt stress, the WT plants accumulated markedly higher levels of O_2.-, H_2O_2, and TBARS, whereas the two *OE* lines maintained significantly lower levels of these indicators (Figure 7D–F), indicating that *AhSNAT5* overexpression alleviates ROS accumulation and peroxidation of membrane lipids. In accordance with the reduced ROS levels, the activities of antioxidant enzymes were substantially elevated in the *OE* lines under salt stress. Under salt stress, the activities of SOD, POD, and CAT in *OE1* and *OE5* were significantly higher than those in WT plants (Figure 7G–I). Collectively, these results demonstrate that *AhSNAT5* overexpression confers enhanced salt stress tolerance in *Arabidopsis*, likely through promoting melatonin biosynthesis, reducing ROS accumulation, and strengthening antioxidant defense capacity.

3.8. Silencing of AhSNAT5 Compromises Salt Stress Tolerance in Peanut

To further verify the function of *AhSNAT5*, a virus-induced gene silencing (VIGS) approach was employed to knock down *AhSNAT5* expression in peanut. The empty *TRV-00* vector served as the negative control. qRT-PCR analysis showed that the expression of *AhSNAT5* in the silenced plants (*TRV-AhSNAT5*) was reduced to approximately 60% of that in *TRV-00* plants (Figure 8A). Accordingly, the melatonin content in *TRV-AhSNAT5* plants was significantly lower than that in the control (Figure 8B). These results confirmed that silencing *AhSNAT5* substantially suppresses melatonin biosynthesis in peanuts. Furthermore, to assess the effect of *AhSNAT5* silencing on salt stress tolerance, detached leaf discs from *TRV-00* and *TRV-AhSNAT5* plants were subjected to control, salt stress, and salt stress supplemented with exogenous melatonin (25 μm MT) treatments (Figure 8C). Under control conditions, leaf discs of both genotypes remained green, and no obvious difference was observed. After salt treatment, the leaf discs of *TRV-AhSNAT5* plants turned markedly more yellow and chlorotic than those of *TRV-00*, indicating more severe damage. Notably, when exogenous melatonin was applied together with salt, the chlorotic phenotype of *TRV-AhSNAT5* leaf discs was visibly alleviated.

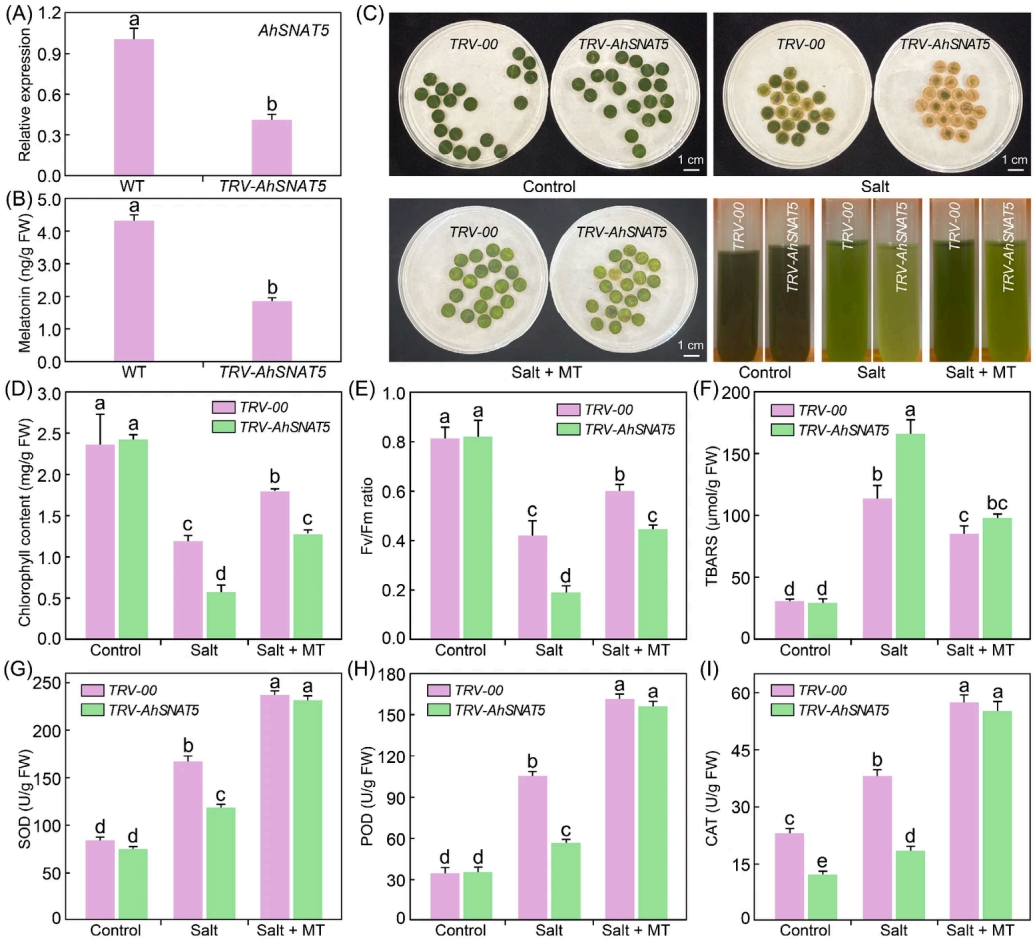


Figure 8. Functional verification of *AhSNAT5* in peanut by virus-induced gene silencing (VIGS). (**A**) Relative expression levels of *AhSNAT5* in *TRV-00* (empty vector control) and *TRV-AhSNAT5* (silenced) peanut plants, determined by qRT-PCR. (**B**) Melatonin contents in *TRV-00* and *TRV-AhSNAT5* plants. (**C**) Phenotypes of detached leaf discs from *TRV-00* and *TRV-AhSNAT5* plants under control, salt stress (200 mM NaCl), and salt stress supplemented with exogenous melatonin (Salt + 25 μm MT) treatments. (**D**–**I**) Chlorophyll content (**D**), *Fv/Fm* ratio (**E**), TBARS content (**F**), and the activities of superoxide dismutase (SOD) (**G**), peroxidase (POD) (**H**), and catalase (CAT) (**I**) in leaf discs of *TRV-00* and *TRV-AhSNAT5* plants under the three treatments. FW, fresh weight. Scale bars = 1 cm. The results are shown as the mean ± SD of three biological replicates. Different lowercase letters above the bars denote significant differences (one-way ANOVA with Tukey's post hoc test, $p < 0.05$).

Consistent with the phenotypic observations, physiological and biochemical analyses further supported these conclusions. Under control conditions, the chlorophyll content and Fv/Fm ratio were comparable between the two genotypes. Salt stress caused a more pronounced decline in chlorophyll content and *Fv/Fm* ratio in *TRV-AhSNAT5* plants than in *TRV-00*. Exogenous melatonin partially restored both parameters in the silenced plants (Figure 8D,E). Similarly, TBARS accumulation was considerably greater in *TRV-AhSNAT5* plants than in *TRV-00*, whereas MT treatment reduced TBARS accumulation in both genotypes (Figure 8F). With respect to antioxidant capacity, the SOD, POD, and CAT activities of *TRV-AhSNAT5* plants were significantly lower than those of *TRV-00* under salt stress. Exogenous melatonin restored the activities of all three enzymes in *TRV-AhSNAT5* plants to levels comparable with those of *TRV-00* (Figure 8G–I). Taken together, these results demonstrated that AhSNAT5 positively regulates salt stress tolerance in peanut by promoting melatonin biosynthesis and enhancing antioxidant capac-

ity, and that exogenous melatonin can partially compensate for the loss of *AhSNAT5* function.

4. Discussion

Melatonin (N-acetyl-5-methoxytryptamine) is a pleiotropic indolamine that functions as a potent antioxidant and signaling molecule in plants [38,39], yet the biosynthetic genes underlying its accumulation in peanut remain largely unexplored. In the present study, we performed the genome-wide identification and characterization of the serotonin N-acetyltransferase (*SNAT*) gene family in peanut (Figure 1). In total, 11 *AhSNAT* genes were identified and comprehensively analyzed at the levels of sequence architecture, evolution, transcriptional regulation, and function. Integrative analysis combining in silico prediction, salt-responsive expression profiling, and genetic manipulation (overexpression in *Arabidopsis* and VIGS-mediated silencing in peanut) established AhSNAT5 as a key regulator of melatonin biosynthesis and salt stress tolerance in peanut.

Structural characterization revealed a high degree of conservation among AhSNAT proteins. All members contained the hallmark Acetyltransf_7 domain with conserved catalytic residues, and motif 1, corresponding to this domain, was present in every AhSNAT protein. Members within the same phylogenetic clade shared highly similar exon-intron organizations and motif compositions (Figure 2), implying that closely related paralogs may retain partially redundant biochemical functions. Moreover, most AhSNAT proteins were predicted to be chloroplast-localized, and the chloroplastic targeting of *AhSNAT5* was experimentally confirmed by transient expression of an *AhSNAT5-GFP* fusion in tobacco leaves (Figure 6B). This observation is consistent with the established notion that plant SNAT enzymes reside in chloroplasts, which are the primary site of melatonin biosynthesis and a major source of stress-induced ROS [40,41]. Chloroplastic localization therefore positions AhSNAT5 at the intersection of melatonin synthesis and the photoprotective response to salt stress. The size of the plant *SNAT* family varies considerably across species, and this variation reflects both lineage-specific expansion and genome evolutionary history [18,42]. In contrast to the limited complement of *SNAT* genes reported in rice and *Arabidopsis*, 11 members were identified in peanut, consistent with its segmental allotetraploid genome derived from the A and B diploid progenitors [43]. A comparable situation has been documented in soybean, in which seven *GmSNAT* genes were identified genome-wide [17], whereas an even larger expansion (52 members) was observed in the tetraploid cotton genome [18]. Importantly, four segmental duplication events (*AhSNAT1/5*, *2/7*, *3/9*, *4/10*) were detected in peanut without any tandem duplication (Figure 3A), indicating that segmental duplication, likely coupled with whole-genome duplication of the allotetraploid ancestor, drove the expansion of this family. All duplicated *AhSNAT* pairs exhibited *Ka*/*Ks* values smaller than 1 (Supplementary Table S3), suggesting that purifying selection has maintained the conserved catalytic function of SNAT proteins during evolution. The extensive collinearity between peanut and soybean and the fewer orthologous blocks with *Arabidopsis* or rice further corroborate the closer phylogenetic affinity of leguminous species.

The diversity of *cis*-acting elements provides a mechanistic framework for understanding the transcriptional complexity of genes [44,45]. The promoters of *AhSNAT1*, *AhSNAT3*, and *AhSNAT9* were enriched in MeJA-responsive elements, whereas those of *AhSNAT2*, *AhSNAT4*, and *AhSNAT7* contained abundant ABA-responsive elements, suggesting potential crosstalk between melatonin biosynthesis and jasmonate or ABA signaling. Meanwhile, the widespread occurrence of defense/stress, anaerobic induction, wounding, drought-, and low-temperature-responsive elements implies that the family

as a whole is predisposed to environmental regulation (Figure 4). This regulatory plasticity was mirrored by the pronounced organ-specific expression patterns observed across leaves, roots, pegs, floral organs, nodules, and developing seeds (Figure 5), supporting the notion of subfunctionalization among *AhSNAT* paralogs. Notably, the stress-responsive transcription of *SNAT* genes under salinity has been reported in other species, in which salt stress up-regulated melatonin biosynthetic genes, including *SNAT*, *TDC*, *T5H*, and *ASMT* [3]. Among the 11 *AhSNAT* genes, *AhSNAT5* stood out as a salt-inducible gene with prominent root-abundant basal expression and a rapid, strong transcriptional response to NaCl treatment, reaching an approximately 8.8-fold induction at 3 h (Figures 5 and 6A). This expression profile is reminiscent of *VvSNAT1* in grapevine, a salt-inducible *SNAT* gene highly expressed in leaves [15]. The rapid induction kinetics of *AhSNAT5* suggest that it acts in the early phase of salt perception, presumably enabling a swift increase in melatonin biosynthesis prior to the onset of extensive oxidative damage.

The functional importance of *AhSNAT5* was substantiated by complementary gain- and loss-of-function approaches. Overexpression of *AhSNAT5* in *Arabidopsis* elevated endogenous melatonin levels and conferred enhanced salt tolerance, accompanied by reduced accumulation of O_2.-, H_2O_2, and TBARS, as well as significantly higher SOD, POD, and CAT activities (Figure 7). This finding agrees with previous reports demonstrating that ectopic overexpression of *SNAT* genes improves stress tolerance through melatonin accumulation, including *VvSNAT1* in transgenic *Arabidopsis* [15] and *SlSNAT*, which interacts with HSP40 to promote thermotolerance in tomato [16]. Mechanistically, melatonin directly scavenges ROS owing to its electron-rich indole structure, and it indirectly reinforces the enzymatic antioxidant system by up-regulating SOD, POD, and CAT [6]. Conversely, VIGS-mediated silencing of *AhSNAT5* in peanut reduced melatonin content and rendered leaf discs hypersensitive to salt stress, with elevated TBARS accumulation and suppressed antioxidant enzyme activities (Figure 8). Critically, exogenous melatonin partially rescued the salt-sensitive phenotype and restored antioxidant capacity in the silenced plants, demonstrating that the contribution of AhSNAT5 to salt tolerance is primarily melatonin-dependent. This result closely parallels the phenotype of *GhSNAT3D*-silenced cotton, in which reduced melatonin content, antioxidant enzyme activity, and salt tolerance were restored by exogenous melatonin supplementation [18]. The partial rather than complete rescue, together with the existence of 10 additional *AhSNAT* paralogs, implies functional redundancy within the family.

5. Conclusions

In summary, a genome-wide survey of peanut led to the identification of 11 SNAT family members, which were subsequently characterized in terms of phylogeny, gene structure, conserved motifs, and stress responsiveness. Transcriptomic profiling and qRT-PCR revealed that the abundance of several transcripts, including those encoding *AhSNAT1*, *AhSNAT5*, *AhSNAT6*, *AhSNAT8*, and *AhSNAT10*, was markedly altered upon NaCl exposure. Among them, the induction of *AhSNAT5* was the most pronounced, and its product was further shown to target the chloroplast. Functional evidence highlighted the central role of this gene in stress adaptation. Specifically, heterologous expression of *AhSNAT5* in *Arabidopsis* promoted endogenous melatonin accumulation and strengthened plant performance under salinity, whereas knockdown of the ortholog via VIGS depressed melatonin biosynthesis in peanut leaves and rendered detached leaf discs more vulnerable to salt challenge. Collectively, these observations deepen our knowledge of how peanut plants perceive and cope with saline conditions and identify *AhSNAT5* as a potential candidate for marker-assisted breeding programs aimed at developing salt-re-

silient cultivars, while further validation across diverse peanut germplasm and under field saline conditions is still required. It should be noted that all functional assays in this study were performed under controlled growth-chamber conditions. Field validation and evaluation of agronomic traits such as pod yield under saline field environments remain to be explored in future investigations. Additionally, ion homeostasis (Na^+ and K^+ accumulation) was not determined in this work, and further experiments are needed to dissect whether AhSNAT5-mediated melatonin modulates ion balance under salt stress.

Supplementary Materials: The following supporting information can be downloaded at https://www.mdpi.com/article/doi/s1. Table S1: Primers in this study; Table S2: List of the *AhSNATs* identified in this study; Table S3: *Ka*/*Ks* ratio of *AhSNATs* replication gene pairs; Table S4: One-to-one *SNAT* orthologous relationships between peanut and other three plant species.

Author Contributions: Conceptualization, G.Z. and Q.W.; methodology, Q.W.; software, F.M.; validation, L.L. and Q.W.; formal analysis, F.M.; investigation, L.L., F.M. and Q.W.; writing—original draft preparation, Q.W.; writing—review and editing, G.Z.; supervision, G.Z.; funding acquisition, G.Z. and Q.W. All authors have read and agreed to the published version of the manuscript.

Funding: This research was funded by the National Natural Science Foundation of China (32301958) and the Shandong Natural Science Foundation (ZR2021QC161 and ZR2023QC057).

Data Availability Statement: All data supporting the findings of this study are available within the paper and within its Supplementary Materials published online.

Conflicts of Interest: The authors declare no conflicts of interest.

References

1. Ismail, A.M.; Horie, T. Genomics, Physiology, and Molecular Breeding Approaches for Improving Salt Tolerance. *Annu. Rev. Plant Biol.* **2017**, *68*, 405–434. [Google Scholar] [CrossRef] [PubMed]
2. van Zelm, E.; Zhang, Y.; Testerink, C. Salt Tolerance Mechanisms of Plants. *Annu. Rev. Plant Biol.* **2020**, *71*, 403–433. [Google Scholar] [CrossRef] [PubMed]
3. ElSayed, A.I.; Boulila, M.; Rafudeen, M.S.; Mohamed, A.H.; Sengupta, S.; Rady, M.; Omar, A.A. Melatonin Regulatory Mechanisms and Phylogenetic Analyses of Melatonin Biosynthesis Related Genes Extracted from Peanut under Salinity Stress. *Plants* **2020**, *9*, 854. [Google Scholar] [CrossRef] [PubMed]
4. Qi, J.; Song, C.P.; Wang, B.; Zhou, J.; Kangasjärvi, J.; Zhu, J.K.; Gong, Z. Reactive oxygen species signaling and stomatal movement in plant responses to drought stress and pathogen attack. *J. Integr. Plant Biol.* **2018**, *60*, 805–826. [Google Scholar] [CrossRef] [PubMed]
5. Khan, T.A.; Fariduddin, Q.; Nazir, F.; Saleem, M. Melatonin in business with abiotic stresses in plants. *Physiol. Mol. Biol. Plants* **2020**, *26*, 1931–1944. [Google Scholar] [CrossRef] [PubMed]
6. Arnao, M.B.; Hernández-Ruiz, J. Melatonin: A New Plant Hormone and/or a Plant Master Regulator? *Trends Plant Sci.* **2019**, *24*, 38–48. [Google Scholar] [CrossRef] [PubMed]
7. Ahammed, G.J.; Li, Z.; Chen, J.; Dong, Y.; Qu, K.; Guo, T.; Wang, F.; Liu, A.; Chen, S.; Li, X. Reactive oxygen species signaling in melatonin-mediated plant stress response. *Plant Physiol. Biochem.* **2024**, *207*, 108398. [Google Scholar] [CrossRef] [PubMed]
8. Wei, J.; Li, D.X.; Zhang, J.R.; Shan, C.; Rengel, Z.; Song, Z.B.; Chen, Q. Phytomelatonin receptor PMTR1-mediated signaling regulates stomatal closure in *Arabidopsis thaliana*. *J. Pineal Res.* **2018**, *65*, e12500. [Google Scholar] [CrossRef] [PubMed]
9. Zhan, H.; Nie, X.; Zhang, T.; Li, S.; Wang, X.; Du, X.; Tong, W.; Song, W. Melatonin: A Small Molecule but Important for Salt Stress Tolerance in Plants. *Int. J. Mol. Sci.* **2019**, *20*, 709. [Google Scholar] [CrossRef] [PubMed]
10. Li, J.; Liu, J.; Zhu, T.; Zhao, C.; Li, L.; Chen, M. The Role of Melatonin in Salt Stress Responses. *Int. J. Mol. Sci.* **2019**, *20*, 1735. [Google Scholar] [CrossRef] [PubMed]
11. Kang, S.; Kang, K.; Lee, K.; Back, K. Characterization of tryptamine 5-hydroxylase and serotonin synthesis in rice plants. *Plant Cell Rep.* **2007**, *26*, 2009–2015. [Google Scholar] [CrossRef] [PubMed]
12. Kang, K.; Kong, K.; Park, S.; Natsagdorj, U.; Kim, Y.S.; Back, K. Molecular cloning of a plant N-acetylserotonin methyltransferase and its expression characteristics in rice. *J. Pineal Res.* **2011**, *50*, 304–309. [Google Scholar] [CrossRef] [PubMed]

13. Kang, K.; Lee, K.; Park, S.; Byeon, Y.; Back, K. Molecular cloning of rice serotonin N-acetyltransferase, the penultimate gene in plant melatonin biosynthesis. *J. Pineal Res.* **2013**, *55*, 7–13. [Google Scholar] [CrossRef] [PubMed]
14. Byeon, Y.; Lee, H.Y.; Lee, K.; Park, S.; Back, K. Cellular localization and kinetics of the rice melatonin biosynthetic enzymes SNAT and ASMT. *J. Pineal Res.* **2014**, *56*, 107–114. [Google Scholar] [CrossRef] [PubMed]
15. Wu, Y.; Fan, X.; Zhang, Y.; Jiang, J.; Sun, L.; Rahman, F.U.; Liu, C. *VvSNAT1* overexpression enhances melatonin production and salt tolerance in transgenic *Arabidopsis*. *Plant Physiol. Biochem.* **2021**, *166*, 485–494. [Google Scholar] [CrossRef] [PubMed]
16. Wang, X.; Zhang, H.; Xie, Q.; Liu, Y.; Lv, H.; Bai, R.; Ma, R.; Li, X.; Zhang, X.; Guo, Y.D.; et al. SlSNAT Interacts with HSP40, a Molecular Chaperone, to Regulate Melatonin Biosynthesis and Promote Thermotolerance in Tomato. *Plant Cell Physiol.* **2020**, *61*, 909–921. [Google Scholar] [CrossRef] [PubMed]
17. Kumar, G.; Arya, M.; Radhika, P.; Giridhar, P. Genome-wide identification, characterization of Serotonin N-acetyltransferase and deciphering its importance under development, biotic and abiotic stress in soybean. *Int. J. Biol. Macromol.* **2022**, *220*, 942–953. [Google Scholar] [CrossRef] [PubMed]
18. Zhang, Y.; Rui, C.; Fan, Y.; Xu, N.; Zhang, H.; Wang, J.; Sun, L.; Dai, M.; Ni, K.; Chen, X.; et al. Identification of *SNAT* Family Genes Suggests *GhSNAT3D* Functional Reponse to Melatonin Synthesis Under Salinity Stress in Cotton. *Front. Mol. Biosci.* **2022**, *9*, 843814. [Google Scholar] [PubMed]
19. Kang, K.; Lee, K.; Park, S.; Kim, Y.S.; Back, K. Enhanced production of melatonin by ectopic overexpression of human serotonin N-acetyltransferase plays a role in cold resistance in transgenic rice seedlings. *J. Pineal Res.* **2010**, *49*, 176–182. [Google Scholar] [CrossRef] [PubMed]
20. El-Gebali, S.; Mistry, J.; Bateman, A.; Eddy, S.R.; Luciani, A.; Potter, S.C.; Qureshi, M.; Richardson, L.J.; Salazar, G.A.; Smart, A.; et al. The Pfam protein families database in 2019. *Nucleic Acids Res.* **2019**, *47*, D427–D432. [Google Scholar] [CrossRef] [PubMed]
21. Johnson, L.S.; Eddy, S.R.; Portugaly, E. Hidden Markov model speed heuristic and iterative HMM search procedure. *BMC Bioinform.* **2010**, *11*, 431. [Google Scholar] [CrossRef] [PubMed]
22. Wang, J.; Chitsaz, F.; Derbyshire, M.K.; Gonzales, N.R.; Gwadz, M.; Lu, S.; Marchler, G.H.; Song, J.S.; Thanki, N.; Yamashita, R.A.; et al. The conserved domain database in 2023. *Nucleic Acids Res.* **2023**, *51*, D384–D388. [Google Scholar] [CrossRef] [PubMed]
23. Letunic, I.; Bork, P. 20 years of the SMART protein domain annotation resource. *Nucleic Acids Res.* **2018**, *46*, D493–D496. [Google Scholar] [CrossRef] [PubMed]
24. Wilkins, M.R.; Gasteiger, E.; Bairoch, A.; Sanchez, J.C.; Williams, K.L.; Appel, R.D.; Hochstrasser, D.F. Protein identification and analysis tools in the ExPASy server. *Methods Mol. Biol.* **1999**, *112*, 531–552. [Google Scholar] [CrossRef] [PubMed]
25. Chou, K.C.; Shen, H.B. Plant-mPLoc: A top-down strategy to augment the power for predicting plant protein subcellular localization. *PLoS ONE* **2010**, *5*, e11335. [Google Scholar] [CrossRef] [PubMed]
26. Katoh, K.; Rozewicki, J.; Yamada, K.D. MAFFT online service: Multiple sequence alignment, interactive sequence choice and visualization. *Brief. Bioinform.* **2019**, *20*, 1160–1166. [Google Scholar] [CrossRef] [PubMed]
27. Tamura, K.; Stecher, G.; Peterson, D.; Filipski, A.; Kumar, S. MEGA6: Molecular Evolutionary Genetics Analysis version 6.0. *Mol. Biol. Evol.* **2013**, *30*, 2725–2729. [Google Scholar] [CrossRef] [PubMed]
28. Chen, C.; Chen, H.; Zhang, Y.; Thomas, H.R.; Frank, M.H.; He, Y.; Xia, R. TBtools: An Integrative Toolkit Developed for Interactive Analyses of Big Biological Data. *Mol. Plant* **2020**, *13*, 1194–1202. [Google Scholar] [CrossRef] [PubMed]
29. Wang, Y.; Tang, H.; Debarry, J.D.; Tan, X.; Li, J.; Wang, X.; Lee, T.H.; Jin, H.; Marler, B.; Guo, H.; et al. MCScanX: A toolkit for detection and evolutionary analysis of gene synteny and collinearity. *Nucleic Acids Res.* **2012**, *40*, e49. [Google Scholar] [CrossRef] [PubMed]
30. Librado, P.; Rozas, J. DnaSP v5: A software for comprehensive analysis of DNA polymorphism data. *Bioinformatics* **2009**, *25*, 1451–1452. [Google Scholar] [CrossRef] [PubMed]
31. Wang, Q.; Li, X.; Li, Z.; Sun, Q.; Li, C.; Zhao, X.; Shan, S. Molecular characterization of Pleiotropic Drug Resistance (PDR) genes involved in tolerance of cadmium in peanut (*Arachis hypogaea* L.). *Ecotoxicol. Environ. Saf.* **2024**, *288*, 117324. [Google Scholar] [CrossRef] [PubMed]
32. Wang, Q.; Li, X.; Guo, C.; Wen, L.; Deng, Z.; Zhang, Z.; Li, W.; Liu, T.; Guo, Y. Senescence-related receptor kinase 1 functions downstream of WRKY53 in regulating leaf senescence in *Arabidopsis*. *J. Exp. Bot.* **2023**, *74*, 5140–5152. [Google Scholar] [CrossRef] [PubMed]

33. Livak, K.J.; Schmittgen, T.D. Analysis of relative gene expression data using real-time quantitative PCR and the 2(-Delta Delta C(T)) Method. *Methods* **2001**, *25*, 402–408. [Google Scholar] [PubMed]
34. Zhang, X.; Henriques, R.; Lin, S.S.; Niu, Q.W.; Chua, N.H. *Agrobacterium*-mediated transformation of *Arabidopsis thaliana* using the floral dip method. *Nat. Protoc.* **2006**, *1*, 641–646. [Google Scholar] [CrossRef] [PubMed]
35. Wang, Q.; Zhang, Z.; Guo, C.; Zhao, X.; Li, Z.; Mou, Y.; Sun, Q.; Wang, J.; Yuan, C.; Li, C.; et al. Hsf transcription factor gene family in peanut (*Arachis hypogaea* L.): Genome-wide characterization and expression analysis under drought and salt stresses. *Front. Plant Sci.* **2023**, *14*, 1214732. [Google Scholar] [PubMed]
36. Zhao, X.; Li, C.; Shan, S.; Sun, Q.; Wang, Q. Physiological and Transcriptomic Analyses of Salt Stress Response in Peanut Seedling. *Agronomy* **2026**, *16*, 1836. [Google Scholar] [CrossRef]
37. Shreya, S.; Supriya, L.; Padmaja, G. Melatonin induces drought tolerance by modulating lipoxygenase expression, redox homeostasis and photosynthetic efficiency in *Arachis hypogaea* L. *Front. Plant Sci.* **2022**, *13*, 1069143. [Google Scholar] [CrossRef] [PubMed]
38. Liu, Y.; Wang, X.; Lv, H.; Cao, M.; Li, Y.; Yuan, X.; Zhang, X.; Guo, Y.D.; Zhang, N. Anabolism and signaling pathways of phytomelatonin. *J. Exp. Bot.* **2022**, *73*, 5801–5817. [Google Scholar] [CrossRef] [PubMed]
39. Zeng, W.; Mostafa, S.; Lu, Z.; Jin, B. Melatonin-Mediated Abiotic Stress Tolerance in Plants. *Front. Plant Sci.* **2022**, *13*, 847175. [Google Scholar] [PubMed]
40. Tan, D.X.; Reiter, R.J. An evolutionary view of melatonin synthesis and metabolism related to its biological functions in plants. *J. Exp. Bot.* **2020**, *71*, 4677–4689. [Google Scholar] [CrossRef] [PubMed]
41. Zhou, W.; Yang, S.; Zhang, Q.; Xiao, R.; Li, B.; Wang, D.; Niu, J.; Wang, S.; Wang, Z. Functional Characterization of Serotonin N-Acetyltransferase Genes (SNAT1/2) in Melatonin Biosynthesis of Hypericum perforatum. *Front. Plant Sci.* **2021**, *12*, 781717. [Google Scholar] [PubMed]
42. Zhang, J.; Yao, Z.; Zhang, R.; Mou, Z.; Yin, H.; Xu, T.; Zhao, D.; Chen, S. Genome-Wide Identification and Expression Profile of the SNAT Gene Family in Tobacco (*Nicotiana tabacum*). *Front. Genet.* **2020**, *11*, 591984. [Google Scholar] [PubMed]
43. Leal-Bertioli, S.; Shirasawa, K.; Abernathy, B.; Moretzsohn, M.; Chavarro, C.; Clevenger, J.; Ozias-Akins, P.; Jackson, S.; Bertioli, D. Tetrasomic recombination is surprisingly frequent in allotetraploid *Arachis*. *Genetics* **2015**, *199*, 1093–1105. [Google Scholar] [CrossRef] [PubMed]
44. Schmitz, R.J.; Grotewold, E.; Stam, M. *Cis*-regulatory sequences in plants: Their importance, discovery, and future challenges. *Plant Cell* **2022**, *34*, 718–741. [Google Scholar] [CrossRef] [PubMed]
45. Marand, A.P.; Eveland, A.L.; Kaufmann, K.; Springer, N.M. *c*is-Regulatory Elements in Plant Development, Adaptation, and Evolution. *Annu. Rev. Plant Biol.* **2023**, *74*, 111–137. [Google Scholar] [CrossRef] [PubMed]

Disclaimer/Publisher's Note: The statements, opinions and data contained in all publications are solely those of the individual author(s) and contributor(s) and not of MDPI and/or the editor(s). MDPI and/or the editor(s) disclaim responsibility for any injury to people or property resulting from any ideas, methods, instructions or products referred to in the content.